JOURNAL OF SOLID STATE CHEMISTRY 58, 1–13 (1985)

Electrochemical Investigations of Conductivity and Chemical Diffusion in Pure and Doped Cubic $SrTiO_3$ and $BaTiO_3$

J. MAIER

Max-Planck-Institut für Festkörperforschung, D-7000 Stuttgart, West Germany

G. SCHWITZGEBEL

FB 13.2 Physikalische Chemie der Universität des Saarlandes, D-6600 Saarbrücken, West Germany

AND H.-J. HAGEMANN

Philips GmbH Forschungslaboratorium, D-5100 Aachen, West Germany

Received December 2, 1983; in revised form August 6, 1984

Pure barium and strontium titanate as well as donor (La)- and acceptor (Mn, Fe, Cr)-doped materials were investigated as both ceramics and single crystals. Alternating current and direct current methods using reversible and polarization cells, as well as concentration cells, were applied. The electronic and ionic conductivities, the dielectric constant, and the phase boundary parameters were measured as functions of temperature (700°C) and of oxygen partial pressure (10^1–10^5 Pa). An ionic contribution via internal surfaces was found in $BaTiO_3$ samples. The effective diffusion coefficients of ceramic (10^{-8} cm^2 sec^{-1} at 600–650°C) and single crystalline (10^{-9} cm^2 sec^{-1} at 630–660°C) $BaTiO_3$ were determined. The formulae presented allow the evaluation of the experiments even for the case of defects with variable charges.

Introduction

The defect reactions in the perovskites $MTiO_3$ (M = Sr, Ba) have been investigated by many authors (*1–4*) in order to study basic problems of solid-state chemistry as well as to improve the material properties for special technical purposes. These investigations were performed in the high temperature range (≥900°C), which is important for the manufacturing process. The conductance behavior could be satisfactorily interpreted in terms of Sr and Ba vacancies (V_M, V'_M, V''_M) and with oxygen vacancies (V_O, $V_O^{\cdot}$, $V_O^{\cdot\cdot}$) as dominant ionic point defects (*11*). Because of its surroundings and its high valence, the Ti^{4+} ion is fixed in a deep potential minimum, so that the existence of Ti lattice defects is improbable. Interstitial defects in the perovskite lattice can be excluded for geometrical reasons. The conductance and valence band states can be attributed to the 3*d* orbitals of Ti and the 2*p* orbitals of O, respectively (*15, 16*). Thus, the conductance electrons (e') correspond to Ti^{3+} and the defect electrons ($h^{\cdot}$) to O^-.

0022-4596/85 $3.00

Little attention has been paid to the ionic conductivity of the titanates. Whereas at high temperatures the conductance has been well explained as purely electronic, an almost purely ionic conductance has been found in ceramic $BaTiO_3$ at 250°C by means of concentration cell measurements (*17*). In $SrTiO_3$ a predominantly ionic conductance at low temperatures is assumed in order to interpret the electrocoloration effect of transition metal-doped samples (*18–20*).

The aim of the present work is a consistent analysis of the results, which can be obtained by electrochemical measurements in the temperature range from 500 to 700°C. Besides the establishment of the conductance behavior and the defect model, the analysis comprises the effective diffusion coefficient and the electric phase boundary parameters. Several independent electrochemical techniques were applied, partially for the first time on these semiconductors (polarization measurements, concentration cell experiments, impedance techniques, and dc measurements at different time resolutions). Single crystalline and ceramic materials were compared for two reasons:

(i) The time for reaching equilibrium with the gas atmosphere often exceeds the measuring times in the case of single crystals, but it decreases strongly in the case of polycrystalline substances with small grain sizes.

(ii) The influence of grain boundaries on the conductivity merits special observation.

Experimental

The $BaTiO_3$ single crystal was made from a TiO_2-excess melt (1300–1400°C, air) using the Czochralski method.[1] The starting materials were $BaTiO_3$ obtained from the thermal decomposition of Ba titanyloxalate (Selectipur, Merck) and TiO_2 (Optipur, Merck). The well-grown colorless crystal had a Curie point of 131°C.

The pure and doped $SrTiO_3$ single crystals were purchased from Titanium Pigment Div./NL Industries (South Amboy, N.Y.). According to the manufacturer the crystals were prepared using the Verneuil method (H_2–O_2 (excess) firing at 2100°C) and tempered 15 hr in air at 1500°C. The purity of these crystals was high and the concentration of the impurity elements influencing the properties under consideration was small (1–25 μg/g $SrTiO_3$) (*14*).

For the preparation[2] of the pure and doped ceramic samples, $BaCO_3$, $SrCO_3$ (Selectipur, Merck), rutile (Kronos R 1o53, Deutsche Titangesellschaft), and the dopants $MnCO_3$, Fe_2O_3, Cr_2O_3, or La_2O_3 were mixed in calculated amounts, pulverized in agate mortars, and submitted to reaction sintering (1150°C). The pulverized materials were pressed and sintered again (1350°C) in O_2. The Fe-doped $SrTiO_3$ was first sintered 4 hr at 1470°C in a wet N_2 atmosphere containing 5% H_2 in N_2 and then 4 hr in O_2 at 1200°C (*14*). Some of the samples (see Table I) contain a small excess of TiO_2, which facilitates the sintering process by giving rise to small quantities of a TiO_2-rich melt and by providing dense and hard materials. In $BaTiO_3$ the TiO_2 excess forms a Ti-rich phase $Ba_6Ti_{17}O_{40}$ localized in the grain boundaries (*22*), whereas in $SrTiO_3$ a TiO_2-richer phase does not exist, so that TiO_2 is deposited in the grain boundaries. The impurity concentrations in the ceramic materials are given in (*14*), and are found to be lower than in the starting substances.

In Table I the materials are specified with respect to exact stoichiometry, grain size, and density.

Sample disks (diameter 1 cm; thickness 1

[1] We are indebted to Dr. Albers (Technical Physics, University of Saarbrücken, West Germany), who had produced the crystal (*14, 21*).

[2] Philips Research Laboratories, D-5100 Aachen, West Germany.

TABLE I

PROPERTIES OF THE SAMPLES

Designation	Composition	Grain diameter (μm)	Density (g cm^{-3})
s.c.$BaTiO_3$	$BaTi_{1.01}O_{3+x}$	∞	6.02
cer. $BaTiO_3$	$BaTi_{1.005}O_{3+x}$	20–40	5.67
cer.Cr–$BaTiO_3$	$Ba(Ti_{0.995}Cr_{0.01})O_{3+x}$	10	5.85
cer.Fe–$BaTiO_3$	$Ba(Ti_{0.995}Fe_{0.01})O_{3+x}$	10	5.99
cer.Mn–$BaTiO_3$	$Ba(TiMn_{0.005})O_{3+x}$	10	5.99
s.c.$SrTiO_3$	$SrTiO_{3+x}$	∞	5.11
cer.$SrTiO_3$	$SrTi_{1.005}O_{3+x}$	20–40	4.81
s.c.La–$SrTiO_3$	$(Sr_{0.999}La_{0.001})TiO_{3+x}$	∞	5.11
cer.La–$SrTiO_3$	$(Sr_{0.995}La_{0.005})Ti_{1.005}O_{3+x}$	20–40	4.80
s.c.Mn–$SrTiO_3$	$Sr(Ti_{0.999}Mn_{0.001})O_{3+x}$	∞	5.11
cer.Mn–$SrTiO_3$	$Sr(TiMn_{0.005})O_{3+x}$	20–40	4.95
s.c.Fe–$SrTiO_3$	$Sr(Ti_{0.9977}Fe_{0.0023})O_{3+x}$	∞	5.11
cer.Fe–$SrTiO_3$	$Sr(TiFe_{0.005})O_{3+x}$	30–70	4.99

Note. s.c., single crystal; cer., ceramic.

mm) were cut from the sintered pellets and polished. With the exception of ceramic $BaTiO_3$, Cr–$BaTiO_3$, and $SrTiO_3$ samples (see Fig. 1a) the porosity of the ceramic samples, for which Fig. 1b is representative, was very low (see Table I). The electrodes (diameter 5 mm) on the samples ((001) planes of the single crystals) and on the disks of CaO-doped ZrO_2 (Friedrichsfeld) were prepared using stoved Ag varnish. This was shown in comparison experiments to be just as suitable as sputtered Pt (*23*).

The apparatus, the electrical equipment, and the execution of the measurements have been described elsewhere (*24*).

Measurements and Evaluation

In order to observe ohmic and charge transfer overvoltages, dc polarization was performed by applying a constant current to the cell:

(Cell 1) Ag, $O_2(P^0)|MTiO_3|O_2(P^0)$, Ag.

After having reached the steady state, the circuit was opened and the voltage decay was recorded as the polarization had been previously. In the same manner the concentration polarization of $BaTiO_3$ between electron blocking electrodes ZrO_2 (CaO) was examined in the cell:

(Cell 2) Ag,

$$O_2(P^0)|ZrO_2|BaTiO_3|ZrO_2|O_2(P^0),\ \text{Ag}.$$

The total polarization voltage may be divided into

$$U(t) = U_E(t) + \Sigma U_D(t) + U_o(t) + U_d(t). \quad (1)$$

In the above U_E represents the ohmic polarization of the electrodes: $U_E = I_P R_E (1 - \exp(-t/\tau_E))$; the polarization current is given by $I_P = i_P \times$ (electrode area); $\tau_E = R_E \times C_E$; R_E is the electrode resistance; C_E is the electrode capacitance. The second term in (1) represents the transfer and boundary overvoltages: $\Sigma U_D = I_P \Sigma R_D (1 - \exp(-t/\tau_D))$; $\tau_D = R_D \times C_D$; R_D is the transfer resistance; C_D is the phase boundary capacitance. The third term represents the ohmic polarization of the sample: $U_o = I_P R(1 - \exp(-t/\tau))$; $\tau = R \times C$; R is the sample resistance; C is the sample capacitance. The last term

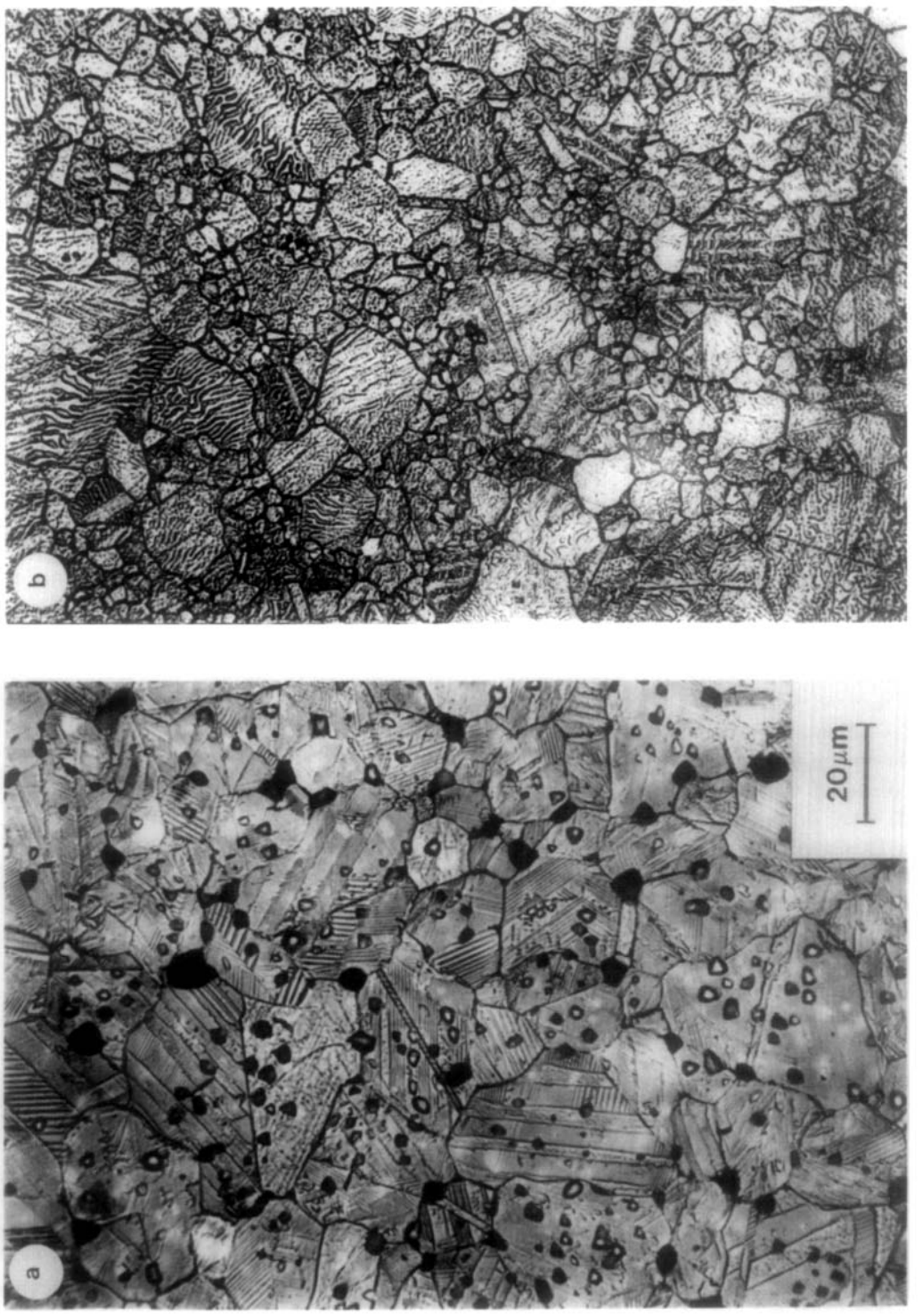

FIG. 1. Metallografic photos of etched (aqueous HCl–HF mixture) surfaces of $BaTi_{1.005}O_{3+x}$ (a) and of $BaTiMn_{0.005}O_{3+x}$ (b).

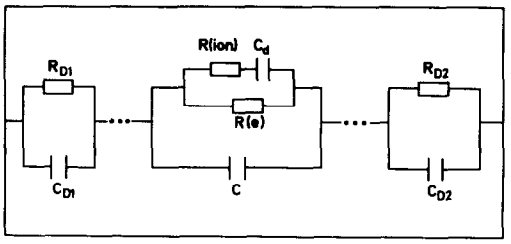

FIG. 2. Equivalent circuit of the electrochemical cells. Electrode (R_D, C_D) and diffusion phenomena (C_d) are taken into account. The insertion of further phases (ZrO_2) is indicated (...).

in (1), $U_d(t)$, represents the concentration polarization.

The simple manner, in which Eq. (1) takes into account the charge-transfer polarization with simultaneous concentration polarization holds only for small transfer impedances (*23*).

At longer times $t > \tau_d/2 \gg \tau_E, \tau_D, \tau$, the Fourier series of U_d is represented by its first terms (*23–25*).

$$U(t) = I_P(R_E + R_D + R) + A[1 - (8/\pi^2)\exp(-t/\tau_d)] \quad (2)$$

with

$$A = \frac{\sigma(e) + \sigma_i(O)}{\sigma} \frac{i_P L}{\sigma(O) + \sigma_i(O) + \frac{2[\sigma_i(O) + 2s(O)]\sigma}{\sigma(e) + \sigma_i(O)}} \quad (3)$$

and

$$s(O) = \frac{F^2}{RT}[D(V_O)c(V_O) + D(O_i)c(O_i)]. \quad (4)$$

Here $\sigma(k)$ is the specific conductivity of k; $\sigma_i(O) = \sigma(V_O^{\cdot}) + \sigma(O_i')$; $\sigma(e) = \sigma(e') + \sigma(h^{\cdot})$; $D(k)$ represent the individual diffusion coefficient of k; and L is the thickness of the sample.

In the steady state ($t \to \infty$) Eq. (2) simplifies to

$$V = I_P(R_E + R_D + R) + A \quad (5)$$

and the decay of the polarized state, the depolarization, obeys

$$U = I_P R_E \exp(-t/\tau_E) + I_P \Sigma R_D \exp(-t/\tau_D) + I_P R \exp(-t/\tau) + A(8/\pi^2)\exp(-t/\tau_d) \quad (6)$$

if $U_d(t)$ is represented by the long-term expression specified in Refs. (*23–25*). In the steady state $R(O)$ may be determined from the equivalent circuit (Fig. 2), which represents the case where $s(O)$, $\sigma_i(O) \ll \sigma(O)$. Under these conditions the relaxation time of the concentration polarization τ_d is given by

$$\tau_d = [R_E + R(O)]C_d \quad (7)$$

Generally

$$\tau_d = L^2/(\pi^2 D^*) \quad (8)$$

is related to the effective diffusion coefficient D^*, defined by

$$\frac{\partial c(O)^*}{\partial t} = D^* \frac{\partial^2 c(O)^*}{\partial x^2}$$

where $c(O)^*$ is the positive deviation of the O component from the "concentration of order" (*25*)

$$c(O)^* = c(O_i'') + c(O_i') + c(O_i) - c(V_O^{\cdot\cdot}) - c(V_O^{\cdot}) - c(V_O). \quad (10)$$

In the above $c(k)$ represents the molar concentration of k.

It has been shown (*23, 25*), that in the case of immobile metal defects, D^* is given by

$$D^* = \frac{1}{8F^2}\{2\sigma_i(O) + 4s(O) + [\sigma(e) - \sigma_i(O)][\sigma(O) + \sigma_i(O)]/\sigma\} \frac{d\mu(O_2)}{dc(O)^*} \quad (11)$$

where $\mu(O_2)$ is the chemical potential of O_2. D^* may be determined from polarization experiments by the plot $\ln|U(t) - U(\infty)|$ vs t, which, at long times, yields a straight line, the absolute slope of which is $1/\tau_d$ (see Eqs. (2) and (5)).

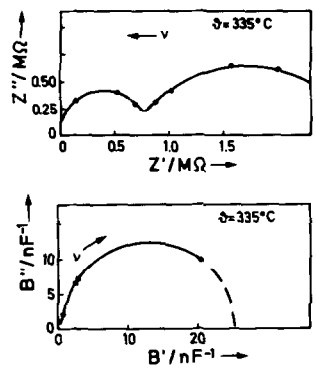

FIG. 3. Complex impedance (Z', Z'') and complex reciprocal capacitance (B', B'') of $SrTiO_3$ (single crystal) in cell 1 ($P(O_2)$ = 20 kPa).

The corresponding expressions for the different impedances may be obtained from the dc voltage by a Laplace transform as shown in (*26*).

In the case of impedance measurements at 100 Hz–10 kHz, and during short-term polarization or depolarization, the concentration polarization is negligible and the equivalent circuit transforms to a series of two parallel R–C links, the elements of which (R, C, $R_D = R_{D1} + R_{D2}$, $C_D = C_{D1}C_{D2}/(C_{D1} + C_{D2})$) can be obtained by fitting the frequency dependence of the complex impedance or by plotting the circle diagrams of the complex impedance and the reciprocal complex capacitance as detailed in Refs. (*23–24*) (see Fig. 3).

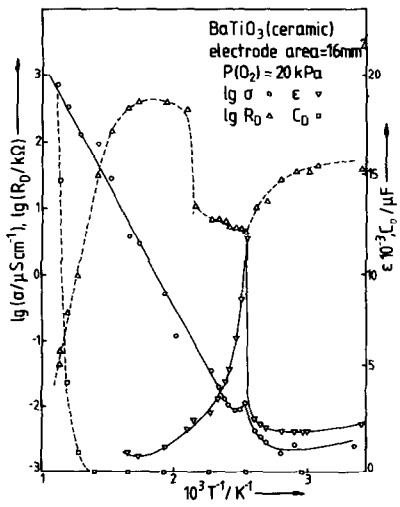

FIG. 4. Specific conductance (σ), dielectric constant (ε), and phase boundary parameters (R_D, C_D) as functions of temperature.

All samples were investigated (350°–700°C; $10–10^5$ Pa) in concentration cells, where the emf (E) is established as

$$E = \frac{\sigma(O) + \sigma_1(O)}{\sigma} \frac{RT}{4F} \ln \frac{P^1}{P^0} \qquad (12)$$

which corresponds to two different partial pressures (P^0, P^1) on the two sides of cell (*1*). Equation (12) includes the conductivity contribution of the singly charged O defects and thus represents a generalization of the usual emf formula for concentration cells.

The Phase Boundary Parameters, R_D and C_D, the Specific Conductivity, and the Dielectric Constant: Results

The R_D–C_D term has its origin mainly in the phase boundaries. This can be concluded from the fact that no particular differences in the parameters R_D and C_D of ceramic and single crystalline specimens were found, apart from La–$SrTiO_3$ (*23*). The temperature dependence of all samples, for which the curves of ceramic $BaTiO_3$ are given as examples in Fig. 4, is very similar to that found for PbO (*24*). The sharp rise of C_D with temperature up to specific values of 1–50 $\mu F/cm^2$ at 600°C is caused by a decrease in the Debye length, which reflects the increasing defect concentrations. The initial rise of R_D is caused by the same effect: the increasing charge concentration enlarges the transfer activation barrier; but this effect is finally overcome by the thermal energy, so that beyond its maximum R_D falls exponentially (*24*). This influence of the electrodes on the two-point measurements on $BaTiO_3$ and $SrTiO_3$, first documented in (*23*), has been recently confirmed by Stumpe *et al.* (*28*). With Pt as an electrode material the specific values of R_D

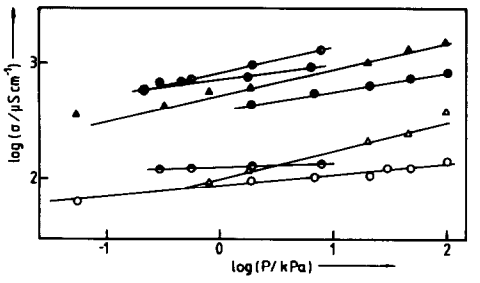

FIG. 5. Pressure dependence of the $BaTiO_3$–materials:

▲	s.c.$BaTiO_3$	600°C
●	cer.$BaTiO_3$	600°C
◐	cer.Fe–$BaTiO_3$	595°C
◓	cer.Cr–$BaTiO_3$	582°C
△	s.c.$BaTiO_3$	500°C
○	cer.$BaTiO_3$	500°C
◒	cer.Mn–$BaTiO_3$	601°C

were higher. The pressure dependences of C_D and R_D are consistent with the interpretation of their T dependence (*23*).

The role of charged defects in the phase boundary is confirmed by the striking behavior of the donator-doped sample La–$SrTiO_3$ where, due to the reduction of $[V_O^{\cdot\cdot}]$ and $[h^{\cdot}]$, C_D and R_D are also diminished (*23*).

The Curie points, taken from the ε curves, were independently confirmed by DTA: For single-crystal $BaTiO_3$, T_C = 131°C; for the ceramic specimens one obtains values of 121°C for $BaTiO_3$, 117°C for Cr–$BaTiO_3$, 94°C for Fe–$BaTiO_3$, and 116°C for Mn–$BaTiO_3$. With the exception of La–$SrTiO_3$ the single crystals obey Curie–Weiss laws in the paraelectric phase. The constants are, for $BaTiO_3$, 1.0×10^5 K; for $SrTiO_3$, 0.9×10^5 K; for Mn–$SrTiO_3$, 1.1×10^5 K; for Fe–$SrTiO_3$, 0.85×10^5 K. The Curie–Weiss temperatures of $BaTiO_3$ (387 K) and $SrTiO_3$ (35 K) are in agreement with the literature (*29–30*).

The Electric Conductivity in Function of Temperature and O_2 Pressure: Results

The specific conductivity σ is determined by the doping and by the preparation conditions. Complete results have been given elsewhere (*23, 27*); here, apart from Fig. 4, only the relative order of the σ values of the different samples between 20 and 400°C is reported. These can be correlated with microstructural and doping properties and with the preparation conditions. One finds that (cer.$SrTiO_3$~) s.c.$BaTiO_3$ ~ cer.Mn–$BaTiO_3$ ~ cer.Cr–$BaTiO_3$ ≪ cer.$BaTiO_3$ ≪ cer.Fe–$BaTiO_3$; cer.La–$SrTiO_3$ < cer.Sr TiO_3 ≪ cer.Mn–$SrTiO_3$ ~ s.c.Mn–$SrTiO_3$ ~ s.c.$SrTiO_3$ < cer.Fe–$SrTiO_3$ ~ s.c.Fe–$SrTiO_3$ ≪ s.c.La–$SrTiO_3$. The pressure dependence of σ is shown in the plots log σ vs log P (Figs. 5 and 6). The slopes of the graphs are $\frac{1}{4}$ for s.c.$BaTiO_3$, cer.Fe–$BaTiO_3$, and all strontium titanate samples, both ceramic and single crystalline. The slopes are lower for cer.$BaTiO_3$ (0.15 at 600°C; 0.10 at 500°C), cer.Mn–$BaTiO_3$ (0.14 at 600°C), and cer.Cr–$BaTiO_3$ (0.05 at 600°C).

The Results of the Concentration Cell Experiments

Cell experiments were performed on all samples over the temperature range 350–

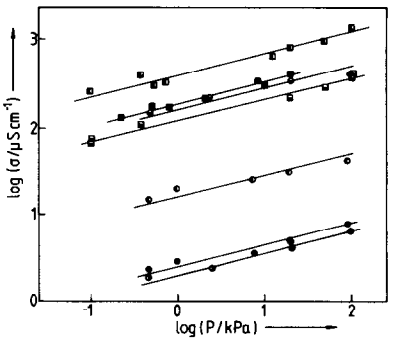

FIG. 6. Pressure dependence of the $SrTiO_3$ materials:

■	s.c.$SrTiO_3$	585°C
◧	s.c.Fe–$SrTiO_3$	568°C
◨	s.c.Mn–$SrTiO_3$	565°C
○	cer.$SrTiO_3$	602°C
◐	cer.Fe–$SrTiO_3$	558°C
◒	cer.Mn–$SrTiO_3$	605°C
◑	cer.La–$SrTiO_3$	600°C

700°C and over the partial pressure range of 10^1–10^5 Pa O_2. With the exception of the ceramic samples $BaTiO_3$ and Cr–$BaTiO_3$, no ionic transport could be detected. Within the accuracy of the measurements this means that

$$t(\text{ion}) \equiv \frac{\sigma(\text{ion})}{\sigma} \leq t(\text{ion})^* \equiv \frac{\sigma(\text{ion}) + \sigma_I(\text{ion})}{\sigma} < 2\%.$$

Four different samples of the same cer.$BaTiO_3$ specimen showed mean t values ranging from 4 to 10%, with very low reproducibility (*23*). Nevertheless, the occurrence of ionic transport of this magnitude was confirmed by exchanging and equalizing the partial pressures P^1 and P^0.

Ionic conductivity increased with $P(O_2)$ in all cases. In some circumstances, especially with cer.$BaTiO_3$, a significant decay with rising temperature was observed.

The results obtained with $BaTiO_3$ are consistent with those of Glower and Heckman (*13*), who for a $BaTiO_3$ ceramic of the same porosity reported that $t(\text{ion}) \simeq 85$–100% (250°C, 1–20 kPa O_2) and $t(\text{ion}) \simeq 7\%$ (550°C, 1–20 kPa O_2); for s.c.$BaTiO_3$ no ionic transport was detected. The same held for s.c.Fe–$BaTiO_3$.

In this work no reliable measurements at $BaTiO_3$ could be made at temperatures lower than 400°C. The success of Glower and Heckman's experiments at 250°C—which they checked by exchanging the partial pressures—can be explained on the basis of a higher exchange current density at this temperature (cf. the temperature profile of R_D in Fig. 4).

Discussion of the Conductance Results

Pure and Acceptor (Mn, Fe) Single Crystals

In the pressure range under consideration the conductance is the p type (*13*), as follows from the P dependence of the purely non-ionic conductivity. It can be supposed (*11*) that O and M vacancies, predominantly in the oxidized form, $V_O^{\cdot\cdot}$ and V_M or V_M'', and the ionized doping ions A_{Ti}' (A = Mn, Cr, Fe) are the major ionic defects. On neglecting valence change processes of the defects, the left-hand side of the electroneutrality equation

$$[A_{Ti}'] + [V_M'] + 2[V_M''] = 2[V_O^{\cdot\cdot}] + [h^{\cdot}] \quad (13)$$

may be regarded as constant, and two extreme cases must then be distinguished:

(i) $[h^{\cdot}] \gg [V_O^{\cdot\cdot}]$. In this case the conductivity ($\sigma \approx \sigma(h^{\cdot})$) does not depend on P.

(ii) $[h^{\cdot}] \ll [V_O^{\cdot\cdot}]$ const. Here, the variation in $[V_O^{\cdot\cdot}]$ according to

$$V_O^{\cdot\cdot} + \tfrac{1}{2}O_2(g) \rightleftharpoons O_O + 2h^{\cdot} \quad (14)$$

is of the same magnitude as the change in $[h^{\cdot}]$, and hence is negligible. The mass action law leads to the result $\partial \log \sigma / \partial \log P = \frac{1}{4}$. This slope was confirmed experimentally. Thus, fully ionized oxygen vacancies, not holes, must be regarded as the mobile majority charge carriers.

Pure and Acceptor (Mn, Fe, Cr)-Doped Ceramics

$BaTiO_3$ ceramics. The experimental results suggest a conductance contribution via internal surfaces. As an approximation we assume an ideally high internal surface density, so that the surface particles (e.g., O_s'') can be formally treated as special crystal defects being in equilibrium with bulk defects, according to

$$O_O + V_s \rightleftharpoons O_s'' + V_O^{\cdot\cdot}. \quad (15)$$

The s sites can be assumed to be in equilibrium with the "grain-boundary phase" discussed in what follows. If charge-transfer processes are neglected, the following charge balance can be formulated:

$$2[V_O^{\cdot\cdot}] - 2[O_s''] + [h^{\cdot}] \simeq \text{const}; \quad (16)$$

the emf for the concentration cell now reads

$$E = \frac{\sigma(V_O^{\cdot\cdot}) + \sigma(O_s'')}{\sigma} \frac{RT}{4F} \ln \frac{P^1}{P^0}. \quad (17)$$

This assumption of ionic transport via internal surfaces is in accordance with all experimental observations (for further arguments see Concentration Polarization of $BaTiO_3$).

(i) The concentration cell measurements fit very well the temperature profile of the results of Glower and Heckmann. The negative temperature coefficient of the ionic transport number is consistent with the low activation energy of surface processes (in contrast to bulk vacancies). Moreover any influence of the small amount of a grain boundary phase, which is present, can be excluded (see below).

(ii) The ionic conductance increases with P; this can be interpreted according to the reaction

$$\tfrac{1}{2}O_2 + V_s \rightleftharpoons O_s'' + 2h^{\cdot} \quad (18)$$

if $[h^{\cdot}]$ is not negligible in Eq. (18), which is independently confirmed by the partial pressure coefficient of the total conductivity.

(iii) According to $N = \partial \log \Sigma\sigma_i = \Sigma t_i \partial \log \sigma_i$ the ionic contribution is negligible to a first approximation at temperatures not lower than 500°C (cf. Fig. 5), as can also be seen from the fact that the slope at fixed temperatures was the same for different values of t(ion). The values for N for cer.$BaTiO_3$, cer.Cr–$BaTiO_3$, and cer.Mn–$BaTiO_3$ samples are smaller than $\frac{1}{4}$, which corresponds to a significant $h^{\cdot}$ concentration. This is consistent with the supposition of an ionic conductivity mechanism via internal surfaces because a $V_O^{\cdot\cdot}$-bulk mechanism would require improbably high mobilities for the bulk defects $V_O^{\cdot\cdot}$. This argument is independent of the manner in which the O_s'' species is taken into account.

(iv) Values of $E > 0$ were only found with cer.$BaTiO_3$ and Cr–$BaTiO_3$ samples of the greatest porosity (5%) (see Fig. 1), i.e., of the greatest internal surface; possibly the ionic transport occurs via pore surfaces rather than grain boundaries. Oxygen surface states of $BaTiO_3$ have been discussed in the literature (*16, 31*). The nonporous cer.Mn–$BaTiO_3$, which is comparable to cer.Cr–$BaTiO_3$ (*14*) in its doping effects, as well as s.c.$BaTiO_3$ show no ionic transport.

(v) This mechanism can explain the striking nonreproducibility. A significant transport of neutral oxygen via open pores would not produce an emf but would still lower the measured voltage with respect to E. This effect could be partially responsible for the poor reproducibility.

The decrease in slope N for BT with decreasing temperature (Fig. 5) is consistent with an increasing ratio $[h^{\cdot}]/[V_O^{\cdot\cdot}]$ (*11*), which is realized because of the activation energies of these defects. This interpretation supports the assumption of exclusively ionic conduction via internal surfaces at low temperatures (*17*) (cf. (i)). At high temperatures it immediately leads to a slope of $\frac{1}{4}$, which has been measured by other authors (*11*) and which is in accord with the expected activation energies. At high temperatures the condition of electroneutrality becomes $[V_O^{\cdot\cdot}]$ = const; thus, Härdtl's explanation of the observed slope of $\frac{1}{4}$(V_{Ba}' and $h^{\cdot}$ as the major defects and both mobile) seems to be questionable. The formation of vacancies by the Schottky reaction

$$M_M + O_O \rightleftharpoons MO + V_M'' + V_O^{\cdot\cdot} \quad (19)$$

undoubtedly reaches equilibrium in the range of the sintering temperature. In the case of $BaTiO_3$ the intermediate BaO probably reacts to form a Ba-rich phase Ba_2TiO_4, or, in the presence of TiO_2 excess (see above) (*22*) the reaction

$$Ba_6Ti_{17}O_{40} + 11BaO \rightleftharpoons 17BaTiO_3 \quad (20)$$

may occur. In the case of single crystals grown from the TiO_2-rich melt (see above) high vacancy concentrations can be ex-

pected, so that for s.c.$BaTiO_3$ the slope $\frac{1}{4}$ should be encountered ($[h^\cdot] \ll [V_O^{\cdot\cdot}]$). In cer.Fe–$BaTiO_3$ the doping metal Fe is predominantly trivalent—in contrast to Cr and Mn—and the high value of Fe'_{Ti} guarantees a purely ionic disorder, resulting in a slope of $\frac{1}{4}$. At the same time, in both series, $BaTiO_3$ and $SrTiO_3$, Fe doping results in the greatest conductivity increase (see above).

$SrTiO_3$ ceramics. Since no Ti-rich phase exists in the system SrO–TiO_3, vacancies in the ceramic $SrTiO_3$ samples probably form by reaction with TiO_2 excess or with impurities; in the single crystals SrO may even evaporate (*11*). In both cases the disorder is purely ionic ($[V_O^{\cdot\cdot}] \gg [h^\cdot]$), but the ionic transport number of the ceramics lies below the measuring limit ($\sigma(h^\cdot) \gg \sigma(V_O^{\cdot\cdot})$). As shown by concentration cell experiments, surface defects O_s'' do not form in contrast to the $BaTiO_3$ ceramics. Insulating TiO_2 even reduces the conductivity of the polycrystalline specimen, compared with the single crystal, whereas in $BaTiO_3$ the situation is reversed. This effect does not appear in the donor materials (see Table I): σ(cer) ~ σ(s.c.) for Fe and Mn–$SrTiO_3$.

Donor (La)-Doped Strontium Titanate

With its valence state ($5d^16s^2$) and its ionic radius (r = 187 pm) La may occupy Sr sites (r = 215 pm), as schematized by

$$La + M_M \rightarrow La_M^\cdot + e' + M. \quad (21)$$

Because in $BaTiO_3$ the enthalpy of the ionization $La_{Ba} \rightleftarrows La_{Ba}^\cdot + e'$ was found to be very low (0.1 eV) (*11*), also, in $SrTiO_3$ totally ionized $La_{Sr}^\cdot$ defects may be assumed to occur. By Eq. (21) the concentrations of both $h^\cdot$ and $V_O^{\cdot\cdot}$ (see Eq. (19)) are diminished (*14*). In cer.La–$SrTiO_3$ the conductivity drops—perhaps favored by the TiO_2 excess—to the lowest level observed in the samples, but it remains p type. M vacancies, moving from the grain boundaries to the bulk, determine the rate of establishment of the defect equilibria. Thus, the grain size in La-doped $BaTiO_3$ has been found to be the effective diffusion length (*13*). The conductivity of s.c.La–$SrTiO_3$ is therefore characterized by strong nonequilibrium effects. A nearly constant electron concentration $[e'] \gg [h^\cdot]$ and a high n conductivity can be assumed because of the reducing atmosphere during preparation (see above). When samples were placed in contact with O_2 the conductivity fell during the experiments because of the formation of low-conductance layers near the surface; minima in the graphs of $\log \sigma = f(\log P)$ were observed (*23*). An analysis of the T dependence of these minima yielded an activation energy of 2.6 eV, whereas the equilibrium value of s.c.$SrTiO_3$ (*6, 31, 32*) is 3.3 eV.

The Concentration Polarization of Barium Titanate

During the polarization experiments with cer.$BaTiO_3$ in cell 2 high contact resistance was observed between the ZrO_2 and the sample pellets. Similar experiments with s.c.$BaTiO_3$ were not practicable. Therefore, cell 2 was modified by inserting a purely ionic conducting liquid lead glass (*23*) as a contact phase between doped ZrO_2 and $BaTiO_3$:

$$\text{(Cell 2a) Ag, } O_2(P^0)|ZrO_2|\underset{P_{x=0}}{\text{glass (l)}}|BaTiO_3|\underset{P_{x=L}}{\text{glass (l)}}|ZrO_2|O_2(P^0), \text{ Ag.}$$

With a conductance in cell 2a of 10–100 μS the polarization experiments could be performed. Samples of cer.$BaTiO_3$ could also be investigated in cell 2a, because the glass phase did not penetrate the grain boundaries, as was confirmed by microscopic and X-ray investigations. The results for cer.$BaTiO_3$ obtained in cells 1 and 2a agreed with each other and in terms of polarization and depolarization. The use of the glass offers other advantages as well:

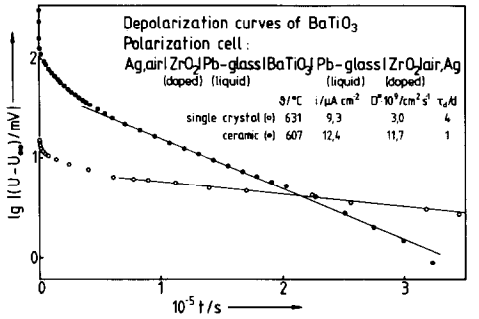

FIG. 7. Determination of the effective diffusion coefficients of $BaTiO_3$ by nonstationary polarization.

(i) Since the liquid glass is a purely ionic conductor no ionic polarization in ZrO_2 is to be expected.

(ii) The contact planes are sealed off from the gas atmosphere, so that O_2 does not interfere. Even the edge can be covered with a thin glass film without providing shunts, as was proved by conductance comparisons.

The polarization currents, chosen in the range of 0.6–14 μA cm^{-2}, led to the different pressure ratios $10 < P_{x=0}/P_{x=L} < 10^4$ at $P^0 = 20.5$ kPa. (In the steady state P^0 is a good approximation to the geometric mean of $P_{x=0}$ and $P_{x=L}$ (*23, 34*).) According to Eqs. (2) and (6), the graphs $\log|U(t) - U(\infty)|$ vs t are linear for long times (Fig. 7). For the single crystal no steady state could be achieved, so that the stationary voltage had to be determined by fitting the curve from its observed section. Nevertheless, the depolarization curve obeyed Eq. (6). From eight measurements on ceramic samples the effective diffusion coefficient, D^*, was found to be (1–4) $\times$ 10^{-8} cm^2 sec^{-1} at 600–650°C, and six measurements on the single crystal yielded $D^* = (3–5) \times 10^{-9}$ cm^2 sec^{-1} at 630–660°C. These results agree satisfactorily with measurements at 900–1200°C (*13*), if extrapolated to 600°C (10^{-8} cm^2 sec^{-1}). Obviously, no insulating grain boundary layers were present in the samples, in contrast to the observations by Schaffrin (*35*) for ceramic specimens prepared in a reducing atmosphere and later exposed to an oxygen-rich atmosphere (*34*). In contrast to the interpretation by this author, it must be concluded that in equilibrated ceramic $BaTiO_3$ diffusion is not hindered by the grain boundaries; his initially highly n-conducting materials (*8, 12*) apparently became insulating as a consequence of a higher transport via internal surfaces (see Eq. (18)). The diffusion coefficient of the ceramic is higher than that of the single crystal, because in the former, grain boundaries contribute to the ionic conductance, as will be considered later. The ionic transference number $t(O)$ can be estimated by analyzing the steady-state voltage. By taking only fully ionized defects into account ($i(O_s') = i(V_O^{\cdot\cdot}) = 0$), the steady-state voltage simplifies to

$$V = I_P(R_E + \Sigma R_D + R(O)). \quad (22)$$

The voltage jump, which accompanies the current switching, in the range $\tau_E, \tau, \tau_D < t \ll \tau_d$ is given by $I_P(R_E + \Sigma R_D + R)$. Because $R(O) \gg R$, R can be neglected in considering the difference between V and the voltage jump; from a.c. measurements one obtains with R that $t(O) = R/R(O)$. The results for the single crystal, $t(O) = t(V_O^{\cdot\cdot}) = 0.5\%$, are poorly reproducible ($\Delta t(O) = 0.3\%$) because V was extrapolated (see above), but the results are compatible with the concentration cell measurements (<2%). For the ceramic both R and $R(O)$ involve both grain boundary as well as bulk effects, so that $t(O) = t(V_O^{\cdot\cdot}) + t(O_s'')$. The results, within 1–2% lie near the lower limit of the emf results. To a first approximation

$$D^*(\text{cer.}) = D^*(\text{s.c.})t(\text{cer.})/t(\text{s.c.}) \quad (23)$$

which explains the difference in D^* values. The good agreement with Eq. (11) is probably accidental, because the equality of the terms $d\mu(O_2)/dc(O)^*$ for both materials represents a very rough approximation.

From Eq. (11) one obtains

$$D^*(\text{s.c.}) = F^{-2}\left\{\frac{\sigma(h^{\cdot})\sigma(V_O^{\cdot\cdot})}{\sigma}\right\}\left\{\frac{d\mu(h^{\cdot})}{d[h^{\cdot}]} + \frac{1}{4}\frac{d\mu(V_O^{\cdot\cdot})}{d[V_O^{\cdot\cdot}]}\right\} \quad (24)$$

and

$$D^*(\text{s.c.}) = t(h^{\cdot})D_F(V_O^{\cdot\cdot}) + t(V_O^{\cdot\cdot})D_F(h^{\cdot}) \quad (25)$$

where $D_F(k)$ denotes the Fick diffusion coefficient of k which is related to the individual diffusion coefficient $D(k)$ according to

$$D_F(k) = D(k)\frac{d \ln a(k)}{d \ln [k]}; \quad (26)$$

here $a(k)$ is the thermodynamic activity of k.

At low defect concentrations, $a(k) \approx [k]$ and $D(k) \approx D_F(k)$. As $t(V_O^{\cdot\cdot}) \ll t(h^{\cdot}) \simeq 1$, Eq. (24) shows that the effective diffusion coefficient essentially describes the $V_O^{\cdot\cdot}$ transport ($D^*(\text{s.c.}) \approx D(V_O)$). The Nernst–Einstein equation

$$4F^2[V_O^{\cdot\cdot}]D(V_O^{\cdot\cdot}) = RT\sigma(V_O^{\cdot\cdot}) \quad (27)$$

can be used for testing the consistency of the interpretation of the D^* value. With $\delta = 5 \times 10^{-3}$ in s.c.$Ba_{1-\delta}\square_\delta TiO_{3-\delta}\Phi_\delta$ (*36*), a very high value being consistent with the conductivity results, the molar mass and the density of $[V_O^{\cdot\cdot}]$ were calculated, and at 900 K ($D^* = 10^{-8}$ cm^2 sec^{-1}), $\sigma(V_O^{\cdot\cdot}) \simeq 10$ μS cm^{-1} was obtained in good agreement with experimental values.

Finally, the equilibration time t_E of O defects in response to changes of the O_2 pressure is estimated. If one imposes a new pressure P^1 at $x = 0$ and $x = L$ on a sample disk (i.e., in cell 2a), which at $t = 0$ had been in equilibrium under the uniform pressure P^0, the solution of Fick's law (*11*) leads to the simple result $t_E = L^2/(2D^*)$. Inserting the values presented here, together with the known values for cer.$SrTiO_3$, one finds that at 900 K for $SrTiO_3$ samples and cer. $BaTiO_3$ materials equilibration requires (1–3) $\times$ 10^5 sec, as was observed experimentally, whereas 6×10^5 sec would have been necessary for s.c.$BaTiO_3$, which was impossible to check for technical reasons. Nevertheless, it could be shown by estimating the theoretical equilibrium conductivities (*23*), that the experimental slopes $\partial \log \sigma/\partial \log P = \frac{1}{4}$ are reliable.

Summary

The main results of the electrochemical investigations can be summarized as follows:

(i) The theory of applied methods has been generalized to include defects with variable charges.

(ii) It is shown that the electrochemical behavior of all cells (phase boundary, ohmic and diffusion processes) can be interpreted in terms of an equivalent circuit.

(iii) The phase boundary properties could be explained as transfer impedances, well known in liquid electrochemistry.

(iv) All bulk conductivity data in the temperature range from 400 to 700°C are consistent with the defect model taking into account $V_O^{\cdot\cdot}$, e', and $h^{\cdot}$ as mobile carriers, while regarding Ba and Sr vacancies, as well as dopant defects, as immobile charge carriers. From the temperature and pressure dependence of the conductivity the high temperature disorder types, which were controversial in the case of $BaTiO_3$, were determined. The gradation of the values and their temperature and oxygen pressure dependence could be explained on the basis of the preparation conditions, the doping effects (Fe'_{Ti}, Mn_{Ti}, Cr_{Ti}, $La^{\cdot}_{Sr}$), and the microstructure.

(v) The bulk conductance in all cases was found to be electronic (p type for pure and acceptor-doped materials at 10^1–10^5 Pa). Nevertheless, in Sr titanates the disorder is purely ionic, whereas in pure cer.$BaTiO_3$ a mixed electronic and ionic disorder was observed, the electronic part of which de-

creases with temperature. This tendency leads to a purely ionic disorder type at high temperature.

(vi) The low temperature ionic conductance, which was found in cer.$BaTiO_3$, is caused by ionic defects (O_s), which are localized at inner surfaces.

(vii) The ambipolar diffusion coefficient in this material is enhanced compared to that of single crystals, where the partial conductivity of oxygen vacancies could be determined and shown to correspond to the Nernst–Einstein relation. Whereas in pure and acceptor-doped materials defect concentrations in the oxygen sublattice reach equilibrium within 1 day ($D^* > 5 \times 10^{-8}$ cm^2 sec^{-1}), the donor (La)-doped samples, especially the single crystals, exhibited strong nonequilibration effects.

Acknowledgments

The financial support of the Stipendien-Fonds der Chemischen Industrie and of the Sonderforschungsbereich 130 "Ferroelektrika" is acknowledged. Discussions with K. H. Härdtl and R. Wernicke are gratefully acknowledged.

References

1. S. A. Long and R. N. Blumenthal, *J. Amer. Ceram. Soc.* **54,** 235 (1971).
2. A. M. S. Seuter, *Philips Res. Rep.*, Suppl. No. 3 (1974).
3. N. H. Chan and D. M. Smyth, *J. Electrochem. Soc.* **123,** 1584 (1976); **128,** 1762 (1981).
4. N. G. Eror and D. M. Smyth, *J. Solid State Chem.* **24,** 235 (1978).
5. N. H. Chan, R. H. Sharma, and D. M. Smyth, *J. Amer. Ceram. Soc.* **61,** 167 (1978).
6. A. E. Paladino, *J. Amer. Ceram. Soc.* **48,** 476 (1965).
7. U. Balachandran and N. E. Eror, *J. Solid State Chem.* **24,** 235 (1978); **39,** 351 (1981).
8. U. Balachandran and N. E. Eror, *J. Electrochem. Soc.* **129,** 5 (1982).
9. U. Balachandran and N. E. Eror, *J. Amer. Ceram. Soc.* **65,** 426 (1982).
10. L. C. Walters and R. E. Grace, *J. Phys. Chem. Solids* **28,** 239 (1967); **28,** 245 (1967).
11. J. Daniels, K. H. Härdtl, D. Hennings, and R. Wernicke, *Philips Res. Rep.* **31,** 487 (1976).
12. J. Daniels, K. H. Härdtl and R. Wernicke, *Philips Techn. Rdschau* **38,** 1 (1979).
13. R. Wernicke, Dissertation, Aachen (1975).
14. H.-J. Hagemann, Dissertation, Aachen (1980).
15. J. W. Schultze and S. Mohr, *in* "Elektrochemie und Elektronik" (D. Behrens, Ed.), p. 231, Verlag Chemie, Weinheim (1981).
16. R. Courths, *in* "SFB 130 Ferroelektrika, Bericht 1980–1982," p. 245, Saarbrücken (1982).
17. D. D. Glower and R. C. Heckman, *J. Chem. Phys.* **41,** 872 (1964).
18. J. Blanc and D. L. Staebler, *Phys. Rev. B* **4,** 3548 (1971).
19. S. L. Mohapatra and S. Wagner, *J. Appl. Phys.* **50,** 5001 (1979).
20. B. W. Foughan and Z. J. Kiss, *IEEE J. Quantum Electron.* **OE-5,** 17 (1969).
21. J. Albers, *in* "SFB 130 Ferroelektrika, Bericht 1974–1976," p. 151, Saarbrücken (1976).
22. R. Wernicke, *Philips Res. Rep.* **31,** 526 (1976).
23. J. Maier, Dissertation, Saarbrücken (1982).
24. J. Maier and G. Schwitzgebel, *Mater. Res. Bull.* **18,** 601 (1983); **17,** 1061 (1982).
25. J. Maier and G. Schwitzgebel, *Phys. Status Solidi B* **113,** 535 (1982).
26. J. Maier, manuscript.
27. J. Maier, Diplomarbeit, Saarbrücken (1979).
28. R. Stumpe, D. Wagner, and D. Bäuerle, *Phys. Status Solidi A* **75,** 143 (1983).
29. T. Sakudo and U. Unoki, *Phys. Rev. Lett.* **26,** 851 (1971).
30. G. A. Samara, *Phys. Rev.* **151,** 378 (1966).
31. W. Heywang, *Solid-State Electron.* **3,** 51 (1961).
32. M. I. Cohen and R. F. Blunt, *Phys. Rev.* **94,** 724 (1954).
33. T. A. Noland, *Phys. Rev.* **94,** 724 (1954).
34. J. Maier, *J. Phys. Chem. Solids,* in press.
35. C. Schaffrin, *Phys. Status Solidi A* **35,** 79 (1976).
36. G. Schwitzgebel *in* "SFB 130 Ferroelektrika, Bericht 1977–1979," p. 260, Saarbrücken (1979).